International Journal of Computer Information Systems and Industrial Management Applications
ISSN 2150-7988 Volume 17 (2025) pp. 1-20

https://doi.org/10.70917/ijcisim-2025-0232
Article

Research on multi-objective optimization design method for automobile suspension based on distributed algorithm

Xing Liu *

Wuxi Transportation Branch, Jiangsu United Vocational and Technical College, Wuxi, Jiangsu, 214151, China; xingxingleader@126.com

Abstract: With the rapid development of the automobile industry, the ride comfort and maneuverability of automobiles in the process of driving have been paid more and more attention. In order to solve the problem of mutual coupling of automobile suspension smoothness and maneuvering stability, the research constructed a multi-objective optimization model of automobile suspension. The model takes the automobile suspension smoothness and handling stability as the objective function, and the particle swarm algorithm is designed in a distributed manner to obtain a distributed discrete particle swarm algorithm to solve the multi-objective optimization model. After adopting this multi-objective optimization method, the root mean square value of the acceleration in the vertical direction of the body and the maximum body roll angle when the car is steering and driving are reduced by 4.65% and 9.27%, which effectively improves the smoothness of the vehicle and the stability of the high-speed vehicle maneuvering, and provides a reference opinion for the tuning and matching of the suspension stiffness, the stiffness of the transverse stabilizer bar and the damping, and provides a certain basis for the designer to choose the appropriate suspension parameters.

Keywords: multi-objective optimization; distributed algorithm; particle swarm algorithm; automobile suspension

1. Introduction

Suspension is an important component of the car, the car driving, due to road surface unevenness or changes in the vertical load of the wheel, resulting in changes in wheel positioning parameters, will affect the performance of the whole car, a good suspension system not only improves the comfort and safety of the car, but also reduces the dynamic load of the tires on the ground [1-4]. And the vibration isolation effect of automobile suspension system has an important impact on the comfort and safety of automobile driving [5]. The traditional passive suspension system is widely used due to its advantages of simple structure, stable performance and low price [6]. However, the structural parameters such as stiffness and damping of the passive suspension cannot be adjusted during automobile driving, making it unable to adapt to complex road conditions [7-8]. In order to overcome this defect, active and semi-active automotive suspension systems have been proposed, in which active suspension systems are gradually becoming mainstream through real-time suspension parameter adjustments in order to realize vehicle performance improvement [9-11]. For automotive suspension optimization, most of them consider to optimize the body acceleration (AS) as the comfort index of the vehicle, but due to the unity of vehicle comfort and handling stability, the requirements of elastic element stiffness and damper damping parameters are conflicting, and the traditional single-objective optimization is difficult to balance the conflicting indexes, and multi-objective optimization becomes a breakthrough of this problem [12-16].

Multi-objective optimization of suspension system, in general, comprehensively considers multi-dimensional parameters such as AS of head or seat, vibration dose value (VDV) of tire dynamic load, and tire deformation (TD), balances parameter conflicts, and seeks for optimal solutions. Literature [17] takes ISO 2631-1 standard as the vehicle ride comfort and health standard, and takes frequency-weighted rms AS, VDV of the head, rms suspension space, and rms TD as the evaluation

indexes, and adopts genetic algorithm (GA) to adjust the proportional-integral-derivative (PID) control parameter and the fuzzy logic control (FLC) membership function, so as to reduce the relevant indexes to achieve a better vehicle comfort and health standards. Literature [18] optimized the ride comfort and vehicle exercise stability of the suspension using multi-objective GA using jitter in vehicle response as the design criterion, and introduced a ranking algorithm considering dissipated energy and vibration control performance to seek the optimal solution from the multi-objective optimization scheme. Literature [19] designed a numerical computational procedure based on non-dominated sorting GA-II (NSGA-II) with vertical dynamic analysis in the time domain, which simultaneously optimizes the two objectives of ride comfort and safety of a suspension system driving under random road contours. Due to higher stiffness and damping coefficient of the suspension better maneuverability can be obtained, but lower damping coefficient can achieve good ride comfort. Literature [20] used the method of approximate ideal solution sequencing (TOPSIS) to determine the optimal range of stiffness and damping of the suspension while reducing the maximum AS and displacement of the springs to complete the multi-objective optimization of the suspension system. Literature [21] used the minimum processing time and stability as the evaluation criteria, listed the pitch center height, equivalent steering stiffness, and lateral steering coefficient of the suspension as the optimization parameters, and used insight sensitivity analysis to determine multiple evaluation indexes such as driver burden, vehicle skid hazard, rollover hazard, and dynamic performance for multi-objective optimization of the vehicle suspension. Literature [22] conducted a multi-objective lightweight optimization of two suspension components (control arm and torsion beam) by means of Kriging model and NSGA-II algorithm under consideration of fatigue life, stiffness, and modal frequency of the suspension components, which resulted in a weight reduction of more than 0.5 kg after optimization. Literature [23] adjusted the stiffness and damping coefficients of damping springs under consideration of dynamic deformation of suspension and dynamic loads, and used adaptive particle swarm algorithms to optimize the AS (vertical and pitch angles) of the body as well as the vertical impact of the wheel motors, resulting in high ride comfort and safety. Literature [24] used seven objective indexes such as AS, VDV, stiffness, and damping coefficient as optimization variables, and performed multi-objective optimization by NSGA-II algorithm based on PID and FLC, which improved ride comfort and health labeling, and reduced the amplitude of vibration of the suspension system. Literature [25] proposed a multi-objective optimization method for suspension system based on NSGA-II algorithm and entropy weight TOPSIS method to optimize ride comfort and controller energy consumption simultaneously. Literature [26] proposed a multi-objective optimization framework for suspension systems based on computer-aided design tools and computer-aided engineering, which achieves ride comfort, stability and mobility, extended life and safety by minimizing chassis pitch AS, reducing the volume and mass of the suspension system, and decreasing the maximum stresses, respectively. Literature [27] constructed a suspension parameter tuning simulation test bed to optimize stiffness and damping coefficients with the help of NSGA-II algorithm to improve ride comfort and stability by testing three ride comfort metrics and two deformation objective functions. Most of the above methods use NSGA-II algorithm and TOPSIS method, which have some defects. In multi-objective optimization problems, the NSGA-II algorithm has high computational complexity, insufficient diversity is maintained, and a variety of parameters need to be adjusted, while the TOPSIS method relies on the influence of weight subjectivity [28-29]. In addition, the multi-objective optimization design method for automotive suspension is still a difficult topic to overcome in the characteristics of suspension systems such as parameter volatility and system nonlinearity, as well as transient performance demands and complex environments [30-32].

And literature [33] constructed a comprehensive model by considering the association between electromagnetic excitation of hub motor and vehicle transient dynamics in electric vehicles, identified the key characteristics of electromagnetic excitation and the key influencing factors of vehicle transient dynamics, and optimized these key characteristics and key factors with the help of Particle Swarm Optimization (PSO) algorithm, which reduces the sensitivity of electromagnetic excitation, and also retains the dynamic advantages of the vehicle. However, the traditional multi-objective PSO algorithm is inefficient, for this reason, literature [34] designed a distributed parallel POS algorithm for solving multi-objective and multi-objective large-scale optimization problems. Literature [35] proposed a novel multi-objective quantum POS algorithm for suspension optimization, and compared with NSGA-II algorithm, the multi-objective quantum PSO algorithm provides a better suspension optimization solution. PSO algorithm is essentially a distributed optimization algorithm. It improves the speed of solving large-scale problems by performing global information search through local information and performing parallel computation while optimizing the global [36]. Distributed algorithm (DA) is an algorithm for solving large-scale optimization problems, which can decompose a large-scale optimization problem into several small-scale subproblems and solve these subproblems by parallel computation to obtain the optimal solution of the original problem [37]. This algorithm has the

characteristics of high efficiency, scalability and fault tolerance, so it has been widely used in the field of distributed computing and multi-objective optimization [38-40]. The application of DA in the optimal design of automobile suspensions, on the other hand, is still in the preliminary exploration stage.

Based on the contradiction between automobile smoothness and maneuvering stability, this paper constructs a multi-objective optimization model of automobile suspension by taking the root-mean-square (RMS) value of the acceleration in the vertical direction of the body and the maximum body inclination angle of the steering vehicle as the indexes of maneuvering stability and smoothness, based on exploring the basic theory of automobile smoothness and the stochastic road generation model, respectively. In order to solve the multi-objective optimization model more efficiently, a distributed structure is introduced into the particle swarm algorithm, and a distributed discrete particle swarm algorithm is designed. Finally, the multi-objective optimization effect of the model is examined by case analysis. The development of this topic can be based on the relevant parameters, the use of computer-aided design in the design stage, an effective and accurate tool for the theoretical prediction and optimization of the car's handling stability and smoothness, thus improving the level of computer-aided design, shortening the development cycle and improving the quality of design.

2. Vehicle smoothness and random road surface generation

2.1. Basic theory of smoothness

2.1.1. Human response to vibration

Mechanical vibration due to its frequency, amplitude, direction and time of action of different, will have a different degree of impact on the human body, at the same time, due to the different physical and psychological tolerance, so each individual response to vibration also has a great difference. For vehicle occupants, the mechanical vibration is divided into local and whole-body vibration.

The human body is composed of a variety of tissues and organs, so in the analysis can be regarded as a vibration system with multiple degrees of freedom, although there are differences between the individuals, but also has its specific inherent frequency. When vibration of different frequencies acts on the human body, the subjective feelings are not the same, so when evaluating the impact of vibration on the human body, the frequency can be used as the basic standard. The human body's response to vibration there are three main resonance zone, 4 to 8Hz for the first resonance zone, 10 to 12Hz for the second resonance zone, 20 to 25Hz for the third resonance zone. The first resonance zone vibration transmitted by the largest energy, the impact on the human body is also the most serious, and with the increase in vibration frequency, the energy transmitted by the gradual attenuation of the trend, the impact on the human body is also reduced accordingly. Human posture also has a great influence on the transmission of vibration. When vibration of the same frequency is applied to the human body, individuals in a standing position will have a weakening effect, while those in a sitting position will have an enhancing effect, especially when the frequency is between 3 and 4.5 Hz, which is the most obvious.

2.1.2. Evaluation method of smoothness

As can be seen from the foregoing, the human body's response to vibration is closely related to both physical and psychological factors, making it difficult to accurately evaluate the smoothness of a vehicle's ride. Currently, subjective and objective evaluation are the two main methods used to evaluate the smoothness of driving.

Subjective evaluation relies on experienced test drivers to actually drive the vehicle and directly evaluate the smoothness of the vehicle by analyzing their intuitive feelings. Objective evaluation takes the frequency, amplitude, acceleration and other physical quantities of vibration as indicators, and quantitatively analyzes the vibration to which the human body is subjected in order to evaluate the smoothness of the entire vehicle. Compared with subjective evaluation, this method does not require test drivers to actually drive the vehicle, so individual differences are excluded from the evaluation results, and there is less human intervention, which helps to more accurately and directly analyze the influencing factors of smoothness, which is also an important reason why this method has been widely used.

2.2. Stochastic pavement generation

2.2.1. Road surface unevenness

The height of a road surface in relation to a reference surface is called the road surface unevenness, which varies according to the road surface direction. Since road surface unevenness is the main cause of vehicle vibration, accurate road surface modeling is the first task to analyze the smoothness of driving.

Since the smooth, random, and various states of experience are the characteristics of the road surface unevenness, it can be analyzed by using the theory of smooth stochastic process. When analyzing the samples taken from the longitudinal section of the road and the road surface of the transaction line, the samples to obtain the power spectral density function (PSD) or variance and other mathematical characteristics to depict the road surface. When the mean value is equal to zero, the power spectral density function can depict the distribution of pavement unevenness energy in the spatial frequency domain, thus demonstrating the structure of pavement waves or pavement unevenness. Therefore, the power spectral density function is an important mathematical feature used to depict the pavement.

The following equation is used as the fitted expression for the pavement power spectral density $G_q(n)$ in the Draft Method for the Representation of Pavement Unevenness in ISO/TC108/SC2N67 as well as in the GB7031 Method for the Representation of Vehicle Vibration Input Pavement Flatness:

$$G_q(n) = G_q\left(n_0\right)\left(\frac{n}{n_0}\right)^{-w} \tag{1}$$

where n is the spatial frequency $\left(m^{-1}\right), n = 1/\lambda, \lambda$ is the wavelength, n_0 is the reference spatial frequency, $n_0 = 0.1\mathrm{m}^{-1}$, $G_q\left(n_0\right)$ is the pavement unevenness coefficient $\left(m^3\right)$, and w is the frequency exponent, which has an important influence on the structure of the pavement power spectral density.

2.2.2. Modeling of pavements

The Ride module in ADAMS/Car provides a pavement profile generator, which is based on Sayers, an empirical model that synthesizes the profile parameters of several types of pavements and also gives the left and right rutting displacements.

The Sayers model has the following equation relationship between the spatial power spectral density G_e and n:

$$G_d(n) = G_e + \frac{G_s}{(2\pi n)^2} + \frac{G_a}{(2\pi n)^4} \tag{2}$$

The right three terms of Eq. are obtained in three independent white noises: G_e is the spatial power spectral density amplitude, G_s is the velocity power spectral density amplitude, and G_a is the acceleration power spectral density amplitude. The three parameters G_e, G_s, G_a are set by the pavement profile generator to generate the desired pavement spectrum.

3. Multi-objective optimization of automobile suspension smoothness and handling stability

Driving smoothness and handling stability as a very important performance in the use of automobiles, this paper proposes a multi-objective optimization method for the suspension system of automobile smoothness and handling stability, using distributed discrete particle swarm algorithm to teach the solution.

3.1. Multi-objective optimization design

Multi-objective optimization design methodology studies the optimization problem with more than one objective function under the given constraints. In a certain sense, the actual optimization problem is generally multi-objective, especially for some complex mechanical design system or the design of the whole machine, often with a variety of design indicators.

The general form of the mathematical model of the multi-objective optimization design problem is:

$$\begin{aligned} &\min F(x) = \left[f_1(x), f_2(x), f_3(x), \ldots\ldots f_m(x)\right]^T \\ &s.t.\ g_i(x) \le 0 \qquad i = 1, 2, \ldots p \\ &h_j(x) = 0 \qquad j = 1, 2, -q \end{aligned} \tag{3}$$

The above general form contains the following problems:

(1) Comparison of two vectors:

Let F^1, F^2 be two m -dimensional vectors:

$$F^1 = \left[F_1^1, F_2^1, F_3^1, \cdots F_m^1\right]^T$$
$$F^2 = \left[F^2{}_1, F_2^2, F_3^2, \cdots F_m^2\right]^T \tag{4}$$

If $F_k^1 = F_k^2 k = 1, 2, \ldots m$, then $F^1 = F^2$.

If $F_k^1 \geq F_k^2 k = 1, 2, \ldots m$ and there is at least one component $F_k^1 > F_k^2$, then $F_k^1 \geq F_k^2$.

If $F_k^1 > F_k^2 k = 1, 2, \ldots m$, call $F^1 > F^2$. Similarly, if $F_k^1 \leq F_k^2 k = 1$, $2, \ldots m$, and at least one component $F^1 < F^2$, call $F_k^1 \leq F_k^2$, and if $F^1 < F^2, k = 1, 2, \ldots m$, call $F^1 < F^2$.

If there exist at least two components F_r and F_s , $F_r^1 > F_r^2$ and $F_s^1 < F_s^2$, then it is said that F^1 , F^2 are not comparable.

(2) Inferior and non-inferior solutions:

For the above multi-objective optimization problem, there are feasible solutions x^0 :

If there exists at least one feasible solution x^1 such that $F\left(x^1\right) \leq F\left(x^0\right)$, then x^0 is said to be an inferior solution.

If there exists no feasible solution x^1 such that $F\left(x^1\right) \leq F\left(x^0\right)$, then x^0 is said to be a non-inferior solution.

(3) Geometric representation of a multi-objective optimization problem:

1) The set of feasible solutions:

$$R = \left\{x \mid g_i(x) \leq 0 i = 1, 2, \ldots p, h_j(x) = 0 j = 1, 2, \ldots q\right\} \tag{5}$$

2) Target set:

$$G = \{F(x) \mid x \in R\} \tag{6}$$

3) like a graph

4) Geometric representation of inferior solutions, non-inferior solutions: one-dimensional unconstrained problems, two-dimensional unconstrained problems, three-dimensional constrained problems.

3.2. Maneuvering Stability Model

The multi-objective optimization model of the whole vehicle considers 10 degrees of freedom, including vertical, pitch, and lateral tilt of the body mass, vertical degrees of freedom of the four wheel masses, lateral motion of the whole vehicle, traverse motion, and rotation of the front wheels around the main pins, and the ones related to the maneuvering stability include lateral tilt of the body mass, lateral motion of the whole vehicle, traverse motion, and rotation of the front wheels around the main pins, etc. The model is designed to provide a model of the steering wheel angle and force input. The maneuvering stability of a vehicle traveling at equal speeds on a smooth road surface is usually investigated by the response to steering wheel angle inputs or force inputs. In order to obtain satisfactory computational accuracy, it is simulated using the appropriate mathematical model. The force and moment balance equations are listed according to D'Alembert's principle, and the moment balance equation for the transverse pendulum motion around the Z axis is obtained as follows:

$$I_z \dot{r} = aF_{yf} - bF_{yr} \tag{7}$$

Where: I_z is the moment of inertia of the vehicle, r is the angular velocity of the pendulum, and F_{yf}, F_{yr} are the lateral deflection force of the front and rear axles, respectively.

Under the action of lateral force, the body tilts sideways around the lateral tilt axis, and the body tilting that occurs when the car is traveling along the curve has a great influence on the handling stability. To establish the mathematical model of the body tilting motion around the X-axis, the differential equations of the body tilting motion are obtained from the moment balance as follows:

$$I_x \ddot{\varphi} - m_s h v(r + \dot{\beta}) = \left(m_s g h - K_{\varphi f} - K_{\varphi r}\right)\varphi - \left(C_{\varphi f} + C_{\varphi r}\right)\dot{\varphi} \tag{8}$$

Where: I_x is the moment of inertia of the car around the X-axis, v is the speed of the center of mass

of the car, β is the lateral deflection angle of the center of mass of the car, m_s is the mass on the spring, φ is the lateral inclination angle of the car body, and h is the lateral inclination force arm, i.e., the difference between the center of mass and the height of the center of lateral inclination on the suspension. $K_{\varphi f}$, $K_{\varphi r}$ are the total lateral camber stiffnesses of the front and rear suspensions, and $C_{\varphi f}, C_{\varphi r}$ are the lateral camber damping of the front and rear suspensions, respectively.

Suspension camber stiffness refers to the total elastic recovery moment of the suspension system to the body under the unit body angle in the case of camber. For the front and rear axles of the car, the total camber stiffness value consists of two parts: the angular stiffness of the suspension spring and the angular stiffness of the lateral stabilizer bar. To wit:

$$\begin{cases} K_{\varphi f} = K_{\varphi f1} + k_{\varphi 1} \\ K_{\varphi r} = K_{\varphi r2} + k_{\varphi 2} \end{cases} \tag{9}$$

Where $K_{\varphi f1}$ is the front suspension spring camber stiffness, $k_{\varphi 1}$ is the front suspension lateral stabilizer bar camber stiffness, $K_{\varphi r2}$ is the rear suspension spring camber stiffness, and $k_{\varphi 2}$ is the rear suspension lateral stabilizer bar camber stiffness. The stiffness of the lateral stabilizer bar is related to its structural arrangement and stabilizer bar diameter. Generally, its arrangement is determined with the arrangement of the whole vehicle, therefore, the adjustment of the lateral stabilizer bar stiffness can only be completed by changing the diameter of the stabilizer bar.

If the linear stiffness of the spring is known, the lateral camber stiffness of the suspension spring can be calculated. For non-independent suspension, the lateral camber stiffness of the suspension spring can be approximated as follows:

$$\begin{cases} K_{\varphi f1} = 0.5 \cdot k_5 \cdot d^2 \\ K_{\varphi r2} = 0.5 \cdot k_6 \cdot d^2 \end{cases} \tag{10}$$

where k_5, k_6 are the front and rear suspension spring line stiffnesses, respectively, and d is the wheelbase. Lateral sway damping refers to the elastic restoring moment given by the suspension to the body system under the unit lateral sway angular velocity in the case of lateral sway, which can be obtained by a similar definition.

Following the force balance equation of lateral motion along the Y-axis, the differential equation of motion for the lateral motion of the car is shown as follows:

$$mu(r + \dot{\beta}) + m_5 h\ddot{\varphi} = F_{yf} + F_{yr} \tag{11}$$

Where: m is the overall vehicle mass and m_5 is the spring loaded mass.

For actual steering system configurations, the steering angle of the wheel becomes another degree of freedom when steering system input is applied to the steering wheel in the form of angular input or torque. The moment balance equation for wheel rotation around the main pin under steering wheel force input:

$$\left[T - I_s(\ddot{\theta} + \dot{r}\cos\alpha - \ddot{\varphi}\sin\alpha)\right] i + F_{yf} D_W - I_W \ddot{\delta} - C_W \dot{\delta} - K_W \delta = 0 \tag{12}$$

Where: T for the steering wheel input torque, I_s for the steering wheel moment of inertia, θ for the steering wheel angle of rotation, α for the steering column and Z-axis angle, i for the steering system ratio, D_W for the tire back to the righting arm, I_W for the front wheels around the main pin moment of inertia, δ for the front wheels, C_W for the coefficient of resistance to the steering force, and K_W for the steering system to the body stiffness.

When the car is traveling normally, the side deflection angle is small, and the side deflection angle and side deflection force are linearly related. The relationship between the side deflection force and the side deflection angle can be written:

$$\begin{cases} F_{yf} = 2k_f \delta_1 \\ F_{yr} = 2k_r \delta_2 \end{cases} \tag{13}$$

where k_f, k_r are the front and rear wheel lateral deflection stiffnesses, and δ_1, δ_2 are the front and rear wheel lateral deflection angles, respectively. From the geometric relationship:

$$\begin{cases} \delta_1 = \beta + \dfrac{a}{v} r - E_f \varphi - \delta \\ \delta_2 = \beta - \dfrac{b}{v} r - E_r \varphi \end{cases} \tag{14}$$

where E_f, E_r are the front and rear wheel roll steering coefficients, respectively.

3.3. Multi-objective optimization model

3.3.1. Objective function

In order to improve the smoothness of vehicle driving, the minimum root mean square value of acceleration in the vertical direction of the body is selected as the first optimization objective; in order to improve the stability of vehicle handling, the minimum maximum body roll angle during steering driving is taken as the second objective function. The objective function is established as follows:

$$\begin{cases} \min f_1(X) = \sigma_{z_s}(X) \\ \min f_2(X) = \max \varphi(X) \end{cases} \tag{15}$$

3.3.2. Design variables

The main function of the suspension system is to transfer the forces and moments acting between the wheels and the frame, and to moderate the impact of the car driving on uneven road surface, attenuate the body vibration caused by it, and ensure the comfort and safety of automobile driving. In view of the influence of suspension spring, lateral stabilizer bar and damper damping parameters on the smoothness and stability of automobile driving, the optimization design variables are selected as:

$$X = \left[k_5, k_6, c_5, c_6, k_{\varphi 1}, k_{\varphi 2} \right] \tag{16}$$

3.3.3. Constraints

The frequency of the vibration system composed of the front and rear suspension springs and their spring mass is one of the main parameters affecting the smoothness of automobile driving. In the suspension design, the body vibration bias frequency is too large, the spring is stiffer, which is not conducive to the improvement of smoothness. Suspension structure arrangement limits the dynamic deflection can not be too large, so the body vibration bias frequency can not be too small.

The rear suspension bias frequencies n_f and n_r should be satisfied:

$$\begin{cases} n_{fL} < n_f < n_{fR} \\ n_{rL} < n_r < n_{rR} \\ N_L < N = n_f / n_r < N_R \end{cases} \tag{17}$$

where $n_f = \dfrac{1}{2\pi}\left(2 \cdot k_5 (a+b) / \left(m_5 \cdot b\right)\right)^{\frac{1}{2}}, n_r = \dfrac{1}{2\pi}\left(2 \cdot k_6 (a+b) / \left(m_5 \cdot a\right)\right)^{\frac{1}{2}}, n_{fR}, n_{fL}$ are the upper and lower bounds of the front suspension bias frequency n_f, n_{rR}, n_{rL} are the upper and lower bounds of the rear suspension bias frequency n_r, respectively and N_R, N_L are the upper and lower bounds of the front and rear suspension bias frequency ratio N, respectively.

The center of mass side deflection β has a high regression coefficient with the driver's subjective evaluation, and its size has a great influence on the handling stability. If the center of mass side deflection is too large, the maneuvering stability becomes worse; if the center of mass side deflection is too small, the steering of the car is not sensitive. The constraint of the center of mass lateral eccentricity is:

$$\beta_L \le \beta \le \beta_R \tag{18}$$

where β_R, β_L are the upper and lower bounds of the center-of-mass lateral deflection angle, respectively.

The understeer gain in the transient maneuvering process is defined as the ratio of the body swing

angular velocity to the front wheel angle. If the understeer gain is too large, the car is easy to turn and skid or roll over; if the understeer gain is too small, the car is not sensitive to the steering wheel input. The transient understeer gain of the car should be satisfied:

$$G_{rL} \le G_r = r / \delta \le G_{rR} \tag{19}$$

where G_{rR} and G_{rL} are the upper and lower bounds of the transient understeer gain G_r of the car, respectively.

Lateral acceleration steering wheel moment gradient is the main evaluation index of force input motion, and it is a parameter that can reflect its steady state characteristics. The lateral acceleration steering wheel moment gradient is statistically derived for various small cars:

$$T_{pL} \le T_p = \frac{T}{a_y} \le T_{pR} \tag{20}$$

where a_y denotes the lateral acceleration, and T_{pR} and T_{pL} are the upper and lower bounds of the gradient of the steering wheel moment of the vehicle's lateral acceleration, T_p, respectively.

The damping ratio ζ is usually used to evaluate the speed of vibration decay. Too large a value of ζ will transmit a large road shock and even cause the vehicle to jump off the ground and lose traction. When the value of ζ is small, the duration of vibration becomes longer, which is unfavorable to the ride comfort. Therefore, there are:

$$\zeta_L \le \zeta = \frac{c}{2\sqrt{k \times m}} \le \zeta_R \tag{21}$$

Where c denotes the damping coefficient of the damper matched with the spring k, and ζ_R and ζ_L are the upper and lower constraints of the damping ratio ζ, respectively.

In summary, the multi-objective optimization model for the handling stability and smoothness of automobile engine mounting system can be established as follows:

$$\min F(X) = \left\{ \sigma_{\ddot{z}_s}(X), \max \varphi(X) \right\} \tag{22}$$

s.t.

$$\begin{aligned}
&n_{fL} < n_f < n_{fR} \\
&n_{rL} < n_r < n_{rR} \\
&N_L < N = n_f / n_r < N_R \\
&\beta_L \le \beta \le \beta_R \\
&G_{rL} \le G_r = r / \delta \le G_{rR} \\
&T_{pL} \le T_p = T / a_y \le T_{pR} \\
&\zeta_L \le \zeta = c / 2\sqrt{k \times m} \le \zeta_R \\
&\mathrm{X} = \left[k_5, k_6, c_5, c_6, k_{\varphi 1}, k_{\varphi 2} \right]
\end{aligned} \tag{23}$$

3.4. Distributed Discrete Particle Swarm Algorithm

In this paper, we improve the teaching of classical particle swarm optimization algorithm and design a distributed discrete particle swarm algorithm, DDMPSO, to solve the multi-objective optimization model of automobile suspension smoothness and handling stability.

3.4.1. Particle Representation and Initialization

In the classical particle swarm optimization algorithm, the solution of the optimization problem is represented by the positions of the particles in the search space, and the velocities of the particles guide the search direction of the particles to find better positions. For the multi-objective optimization problem of automobile suspension smoothness and handling stability, the definitions of particle positions and velocities need to be re-given with respect to the problem characteristics and optimization approach. In this paper, we adopt discrete PSOA and use direct coding to define the position of the particle. The

position of particle i is defined as:

$$X_i = \{x_1, x_2, \ldots, x_n\} \tag{24}$$

where n is the number of nodes and x_i is the position of the particle. When $x_a = x_b$, it means that node a and node b are located in the same position.

In particle swarm optimization algorithm, the speed of the particle directly determines its search direction, the proper definition of the speed can find out the more accurate solution and speed up the convergence process of the algorithm, this paper defines the speed of the particle i as:

$$V_i = \{v_1, v_2, \ldots, v_n\} \tag{25}$$

where the element $v_j (j = 1, 2, \ldots, n)$ is a binary variable taking the value 0 or 1. When $v_j = 1$, the position corresponding to the particle i changes in some way. Conversely, the position corresponding to particle i does not change.

Traditional particle swarm optimization algorithms set an upper limit on the particle velocity to prevent it from flying out of the boundary, however, the particle velocity in this chapter only contains two values, 0 and 1, and the position updated according to this velocity form will not go out of the range, so there is no need to set the maximum velocity.

In order to accelerate the convergence of the algorithm, this paper adopts the label propagation method to initialize the population, i.e., each node determines its own number based on the number of its neighboring nodes. Assume that the set of neighboring nodes of node i is $\Omega(i) = (x_1, x_2, \ldots, x_k)$, and $l(i)$ denotes the position number to which node i belongs. Next, each node in the network is added to the position to which the most of its neighboring nodes belong, and the mathematical representation of the process is:

$$l(i) = \arg\max_r \sum_{j \in \Omega(i)} \delta(l(j), r) \tag{26}$$

When node i and node j belong to the same location, then $\delta(i, j) = 1$ and vice versa, then $\delta(i, j) = 0$. The process is performed iteratively, and in each iteration each node updates its own label using the labels of its physical neighbors. The method is simple in principle and the computational complexity is close to linear, so the algorithm runs very efficiently.

3.4.2. Particle Velocity Update Method

When the particle swarm optimization algorithm is used to solve a multi-objective optimization problem, the positions of the particles can be defined as a n-dimensional vector, where n is the number of nodes in the network. In addition, the velocity of the particles is also represented as a n-dimensional vector, where each element is a value of either 0 or 1, which is used to indicate whether or not adjustments need to be made to the division of the particle positions at that particular node. The classical discrete particle swarm optimization algorithm velocity update formula is as follows:

$$V_i = sig\left[\omega V_i + c_1 r_1 \left(pBest_i \oplus X_i\right) + c_2 r_2 \left(gBest_i \oplus X_i\right)\right] \tag{27}$$

where ω is the inertia weight, c_1 is and c_2 is the learning factor, r_1 and r_2 are two random numbers between 0 and 1, and $\oplus$ denotes the different-or operation between two vectors. From the description, it can be seen that V_i is a binary quantity, so the classical discrete particle swarm optimization algorithms use the sig function to take the binary operation. Suppose there exist vectors $Y_i = \{x_1, x_2, \ldots, x_n\}$ and $X_i = \{x_1, x_2, \ldots, x_n\}$ and that $Y_i = \mathrm{sig}(X_i)$, then:

$$\begin{cases} y_k = 1 \ \text{When } sig(x_k) > random(0,1) \\ y_k = 0 \ \text{When } sig(x_k) \le random(0,1) \end{cases} \tag{28}$$

Here the sig function is defined as follows:

$$sig(x) = \frac{1}{1 + e^{-x}} \tag{29}$$

From equation (27), it can be seen that the velocity of the particle after updating is determined by three factors, including: the velocity of the particle in the last iteration, the relationship between the

position of the particle in the last iteration and the historical optimal position, and the relationship between the position of the particle in the last iteration and the global optimal position. According to Eq. (27) can achieve better particle swarm optimization results, but there are some limitations in its mathematical significance, a detailed theoretical analysis is given next. The part of the sig function in parentheses in Eq. (27) is expressed as follows:

$$\tilde{V}_i = \omega V_i + c_1 r_1 \left(pBest_i \oplus X_i \right) + c_2 r_2 \left(gBest_i \oplus X_i \right) \tag{30}$$

For ease of understanding, Eq. (30) is transformed into an update of the elements in the particle velocity:

$$\tilde{v}_i^m = \omega v_i^m + c_1 r_1 \left(pBest_i^m \oplus x_i^m \right) + c_2 r_2 \left(gBest_i^m \oplus x_i^m \right) \tag{31}$$

where $pBest_i^m \oplus x_i^m = 0$ or 1, and $gBest_i \oplus x_i^m = 0$ or 1. Assuming that the parameters ω, c_1, c_2, r_1 and r_2 are known, the maximum value of equation (31) and the minimum values are respectively:

When:

$$v_i^m = 1, pBest_i^m \oplus x_i^m = 1, gBest_i \oplus x_i^m = 1, \max\left(\tilde{v}_i^m \right) = \omega + c_1 r_1 + c_2 r_2 \tag{32}$$

When:

$$v_i^m = 0, pBest_i^m \oplus x_i^m = 0, gBest_i \oplus x_i^m = 0, \min\left(\tilde{v}_i^m \right) = 0 \tag{33}$$

It can be seen that Eq. (31) takes values in the range $\tilde{v}_i^m \in \left[\min\left(\tilde{v}_i^m \right), \max\left(\tilde{v}_i^m \right) \right] = \left[0, c_1 r_1 + c_2 r_2 \right]$.

In order to correct the velocity update results, this chapter uses the $\tanh$ function instead of the sig function in Eq. (27), and the proposed velocity update formula is as follows:

$$V_i = \tanh\left[\omega V_i + c_1 r_1 \left(pBest_i \oplus X_i \right) + c_2 r_2 \left(gBest_i \oplus X_i \right) \right] \tag{34}$$

where the parameters ω, c_1, c_2, r_1 and r_2 are defined in the same way as in Eq. (27), and the description will not be repeated in the rest of this chapter. Suppose that there exist vectors $Y_i = \left\{ x_1, x_2, \ldots, x_n \right\}$ and $X_i = \left\{ x_1, x_2, \ldots, x_n \right\}$ and that $Y_i = \tanh\left(X_i \right)$, then:

$$\begin{cases} y_k = 1 \text{ When } \tanh\left(x_k \right) > random(0,1) \\ y_k = 0 \text{ When } \tanh\left(x_k \right) \le random(0,1) \end{cases} \tag{35}$$

Here the $\tanh$ function is defined as follows:

$$\tanh(x) = \frac{e^x - e^{-x}}{e^x + e^{-x}} \tag{36}$$

In the $\tanh$ function, $0 \le \tanh(x) < 1$ when the value of x is in the range of $\left[0, c_1 r_1 + c_2 r_2 \right]$. At this point, using Eq. (28) for binary judgment, the binary judgment result will be more accurate when comparing the $\tanh(x)$ values to random numbers in the range (0, 1).

3.4.3. Particle Position Update Method

After obtaining the binary-based velocity estimation, the particle position update method proposed in this chapter is described:

$$X_i^t = \left\{ X_i^t, pBest_i, gBest \right\} \otimes V_i \tag{37}$$

Where the special symbol $\otimes$ is the key to the particle state update process, which directly affects the performance of the algorithm. Suppose the particle position is $X_1 = \left\{ x_{11}, x_{12}, \ldots, x_{1n} \right\}$, the historical optimal position is $pBest_i = \left\{ p_{11}, p_{12}, \ldots, p_{1n} \right\}$, the global optimal position is $gBest_i = \left\{ g_{11}, g_{12}, \ldots, g_{1n} \right\}$, and the velocity is $V = \left\{ v_1, v_2, \ldots, v_n \right\}$, then the operation symbols $\otimes$ uses these positions and velocities to produce a new particle position X_2. The elements in can be defined by the following equation:

$$\begin{cases} x_{2i} = x_{1i} & \text{if } v_i = 0 \\ x_{2i} = Jbest_i & \text{if } v_i = 1 \end{cases} \tag{38}$$

where $Jbest_k^i$ denotes an integer between 1 and n. Assuming that the set containing all neighboring nodes of node i is $N = \{n_1, n_2, \ldots, n_k\}$, then $Jbest_k^i$ can be computed by the following equation:

$$Jbest^i = \underset{r}{\text{argmax}} \left[\omega \sum_{j \in N} \varphi\left(x_{1j}, r\right) + c_1 r_i \sum_{j \in N} \varphi\left(p_{1j}, r\right) + c_2 r_2 \sum_{j \in N} \varphi\left(g_{1j}, r\right) \right] \tag{39}$$

where $\varphi(i, j) = 1$ when $i = j$, otherwise, $\varphi(i, j) = 0$.

Next, theoretical analysis is used to illustrate the effectiveness of the proposed position update method. In the standard PSOA, the updating equations of particle velocity and position are as follows:

$$v_i^j(t+1) = \omega v_i^j(t) + c_1 r_1 \left(pBest_i^j(t) - x_i^j(t) \right) + c_2 r_2 \left(gBest_i^j(t) - x_i^j(t) \right) \tag{40}$$

$$x_i^j(t+1) = x_i^j(t) + v_i^j(t+1) \tag{41}$$

Bringing equation (40) into (41) gives:

$$x_i^j(t+1) = x_i^j(t) + \omega v_i^j(t) + c_1 r_1 \left(pBest_i^j(t) - x_i^j(t) \right) + c_2 r_2 \left(gBest_i^j(t) - x_i^j(t) \right) \tag{42}$$

Unlike the velocity update formula of the standard particle swarm optimization algorithm, the proposed discrete particle swarm optimization algorithm has a velocity update result of 0 or 1. This binary encoding form can effectively prevent the particles from flying out of the boundary without the need to set the maximum velocity threshold to prevent the particles from flying out of the boundary. In addition, since the proposed particle positions are integer encoded, the velocity binary encoding form also facilitates the position solution. However, the velocity binary form of encoding poses a new problem. If only the last iteration position and velocity are used to update the position at the current moment, as in the position update formulation in the discrete particle swarm optimization algorithm:

$$X_i^t = X_i^t \otimes V_i \tag{43}$$

At this point, the process of position updating weakens the influence of historical optimal position and global optimal position on the results. Different from the discrete particle swarm method, the proposed distributed discrete particle swarm algorithm's particle position updating method simultaneously uses variables and parameters such as the particle's last iteration position, velocity, the particle's own historical optimal position, the population's global optimal position, the learning factor, and the inertia weights, which can fully utilize the population advantage of the particle swarm algorithm.

4. Example analysis

4.1. Establishment of the simulation model of the whole vehicle

The whole vehicle dynamics model studied in this thesis is built up in the. The modeling sequence is bottom-up, in the model to establish each component, including the front, the software provides the constraints will be the rear suspension system model, steering system model, tire model, etc., the use of the various components are connected together, while the introduction of external constraints such as road surface to establish the whole vehicle rigid body model. Through the front suspension, steering system, rear suspension, tires and other subsystems are connected to the corresponding constraints on the center of mass to form the whole vehicle simulation model, the relevant parameters of the whole vehicle are shown in Table 1.

Table 1. The parameters of the vehicle.

Full load load (350KG)	Front axle load (140KG) Rear axle load (195KG)	Drive mode	Four-wheel electric drive
Long × wide × high (mm)	2190×1050×900	Wheelbase (mm)	1595
Front wheel pitch	1128 (mm)	Back wheel pitch	1252 (mm)
Front beam	0.2±0.5deg	The outward Angle of the front wheel	1±0.5deg

The inner Angle of the main pin	5±0.5deg	The back Angle of the main pin	3±0.5deg
Front frame form	Double arm	Front suspension stiffness	10100N/m
Rear frame form	Single transverse arm	Rear suspension stiffness	14000N/m

4.2. Simulation of vehicle handling stability

Steady state steering characteristics is an important aspect of the car's maneuvering performance, the steady state steering characteristics of the car can be divided into three types: understeer, neutral steering and oversteer. Oversteering in low speed is good for vehicle adjustment, and understeering in high speed is good for vehicle stabilization.

The dynamic simulation of the whole vehicle is carried out on the road spectrum to analyze the influence of wheel positioning parameters, suspension stiffness and center of mass position on the steering characteristics of the whole vehicle. The driving speed curve of the whole car is shown in Fig. 1, which is the curve measured when the car is on the horizontal road surface, keeping the steering wheel angle unchanged and gradually increasing the speed. The whole car is doing smooth acceleration, with the time and smoothly increase the speed, when t = 50s, the car's traveling speed is close to 30km / h. The car's turning radius curve is shown in Figure 1, and the steering radius curve is shown in Figure 2.

The turning radius curve of the whole vehicle is shown in Fig. 2. It can be seen that the turning radius of the whole vehicle with time firstly changes suddenly to large and then suddenly to small and then smooth, and finally increases slowly. The sudden change is partly due to the fact that the angular velocity of the vehicle is very small and the turning radius is very large before turning. Figure 3 shows the curve of the turning radius of the vehicle with respect to the speed. The turning radius of the whole vehicle is increasing slowly with the increase of speed. The turning radius is basically unchanged until the speed is less than 18km/h, which is neutral steering. The turning radius increases slowly after the speed is greater than 18km/h, which belongs to understeer.

The lateral acceleration change curve is shown in Fig. 4. The lateral acceleration increases with time and the maximum value is -0.65 g. The lateral camber change curve is shown in Fig. 5. It can be seen that the lateral camber increases smoothly from 0deg to 2.57deg and the lateral camber is small. Figure 6 shows the motion trajectory of the center of mass of the whole vehicle. The motion trajectory of the center of mass can visualize the characteristics of understeer.

Simulation analysis conclusion: the original vehicle in the original suspension parameters, can realize the vehicle understeer characteristics, and the carriage side tilt angle is smaller, basically meet the design requirements.

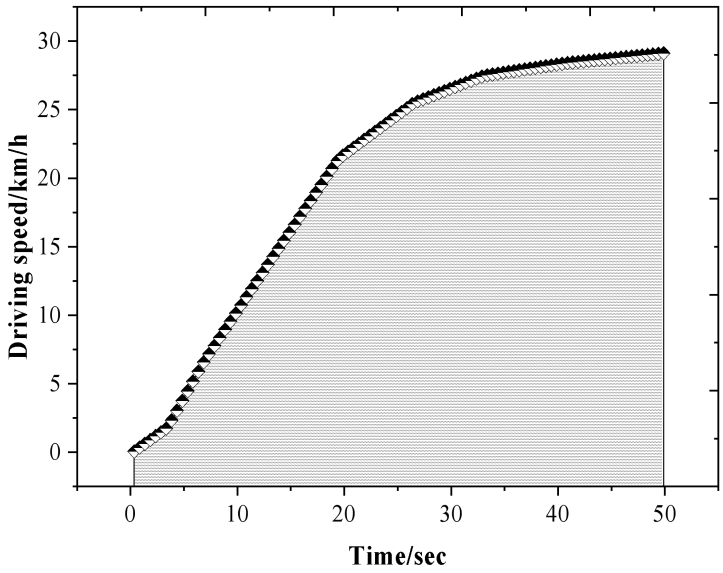

Figure 1. The curve of the car's speed.

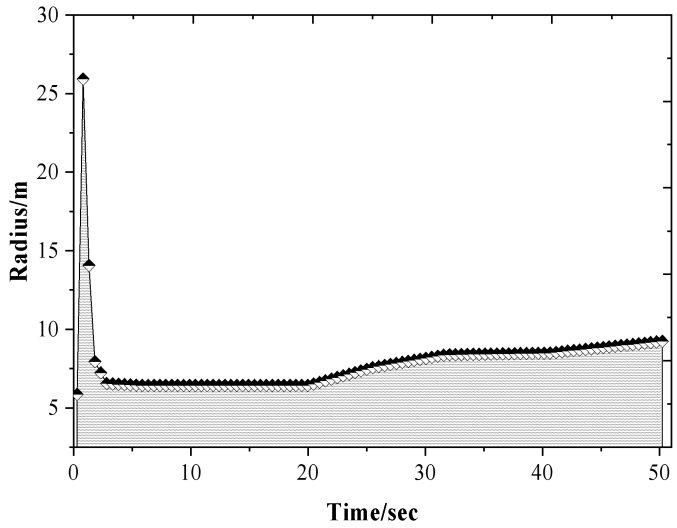

Figure 2. The curve of the turning radius of the vehicle.

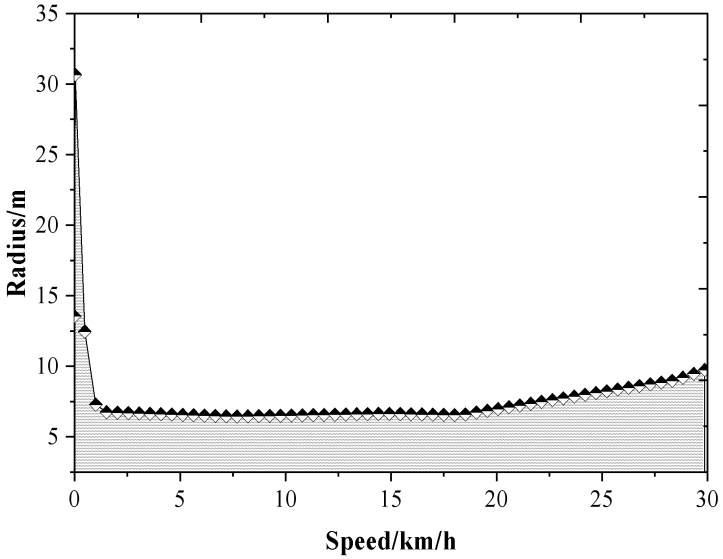

Figure 3. The change curve of the turning radius relative to velocity.

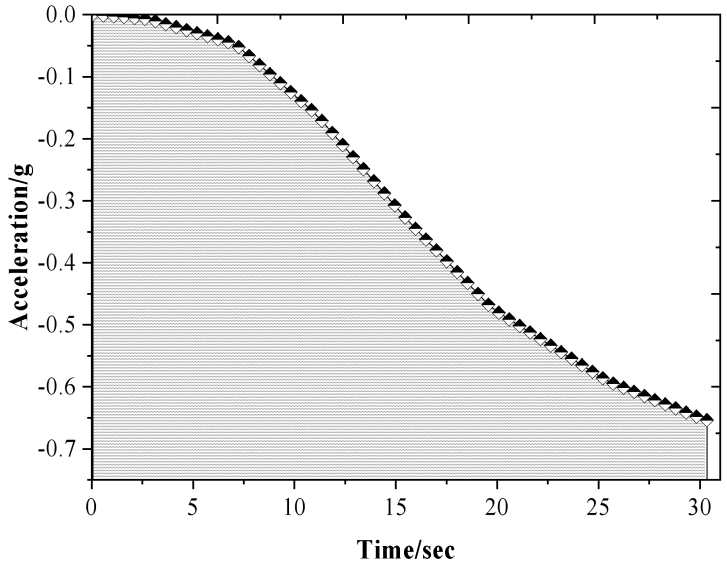

Figure 4. The transition curve of the lateral acceleration.

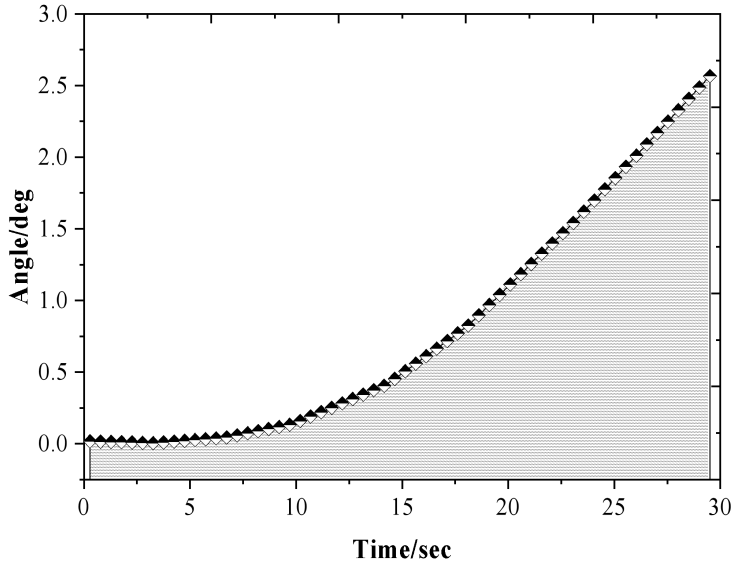

Figure 5. The transition curve of the lateral dip.

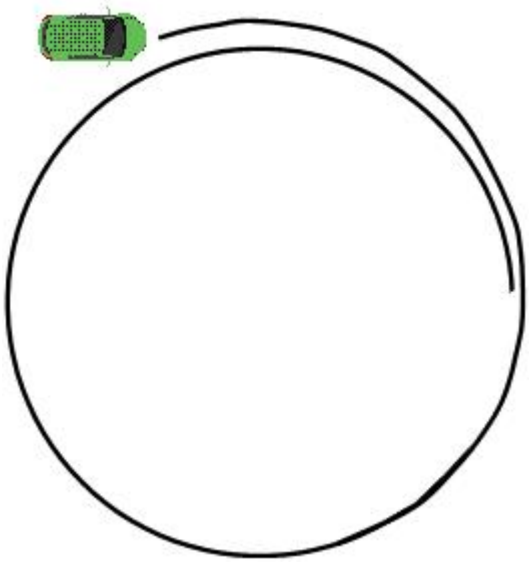

Figure 6. The motion trajectory of the vehicle center.

4.3. Analysis of multi-objective optimization results

The distributed discrete particle swarm algorithm is utilized for solving to obtain the optimal Pareto solution set based on handling stability and smoothness, and a set of better values is selected by comparing the various design results and finally balancing the objectives. Table 2 shows the final optimization results of the design variables and the vehicle performance comparison before and after optimization. The results of the front and rear suspension spring line stiffness, front and rear damper damping coefficients, and total front and rear suspension camber stiffness after optimization are 1.54, 1.53, 1.50, 1.06, 1.14, and 1.08, respectively; the root mean square value of the acceleration in the vertical direction of the bodywork is reduced from 0.43 to 0.41, and the maximum body camber of the car when steering is reduced from 3.56 to 3.23, after optimization. After optimization, the root mean square value of acceleration decreases significantly, which is in a more comfortable range, and at the same time, the body inclination angle decreases after optimization, and the stability and smoothness of the car is enhanced.

Table 2. The performance comparison of vehicle before and after optimization.

Variables	Before optimization	After optimization
Front suspension spring stiffness k_5	1.92	1.54
Rear suspension spring stiffness k_6	1.75	1.53
Front lateral dip stiffness c_5	1.64	1.50
Rear lateral dip stiffness c_6	1.47	1.06
Front suspension damping coefficient $k_{\varphi 1}$	1.56	1.14
Rear suspension damping coefficient $k_{\varphi 2}$	1.45	1.08
The average square root of the acceleration σ_{z_s}	0.43	0.41
Side Angle of car body φ	3.56	3.23

4.4. Evaluation and analysis of experimental results

After modifying the vehicle model according to the suspension parameters obtained from the above optimization method, the validity of the optimization method and the reliability of the optimization results are verified through simulation experiments. The following is a comparison of the results of the smoothness experiment and the handling stability experiment of the car before and after the optimization.

(1) Figures 7 to 9 show the vibration acceleration of the car in three different directions in the smoothness test. The lateral and longitudinal vibration accelerations at the driver's side remain basically

unchanged before and after optimization, while the vertical vibration acceleration is improved.

(2) Fig. 10 shows the variation of the car's transverse pendulum angular velocity in the angular step input experiment. The response time of the transverse pendulum angular velocity is reduced after optimization, so the steering response of the car is more sensitive and rapid.

(3) Figure 11 shows the simulation results of the body lateral inclination angle in the steady-state slewing experiment, and Figure 12 shows the simulation results of the difference between the front and rear axle lateral deflection angles in the steady-state slewing experiment. When the acceleration is 6m/s2, the optimized body lateral inclination angles before and after optimization are -5.74° and -4.89°, respectively, and the body lateral inclination angle is significantly reduced, which improves the vehicle's anti-lateral inclination ability. As seen in Fig. 12, the understeer of the vehicle is also increased.

(4) Figures 13 and 14 show the frequency domain response of the experimental transverse pendulum angular velocity for the steering wheel angle pulse input and the time domain response of the experimental transverse pendulum angular velocity for the steering wheel angle pulse, respectively. From Fig. 13, it can be seen that there is not much change in the resonance peak level before and after optimization, but the resonance peak level (i.e., the increase ratio at resonance) of the vehicle after optimization has been reduced, which makes the vehicle drive more smoothly with different frequency inputs. From Fig. 14, it can be seen that the phase lag angle is almost close to 0 at a frequency of 0.1 Hz, and at a frequency of 1.2 Hz, the time domain response of the pendulum angular velocity is -9.51 and -22.59 before and after optimization, respectively, and the phase lag angle after optimization is reduced, so that the vehicle responds faster when turning the steering wheel rapidly.

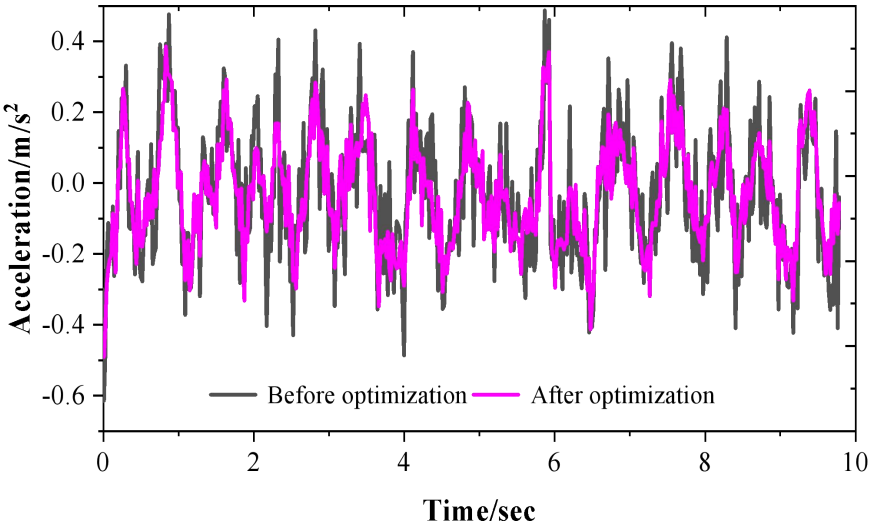

Figure 7. The acceleration curve of vertical vibration at driver's seat.

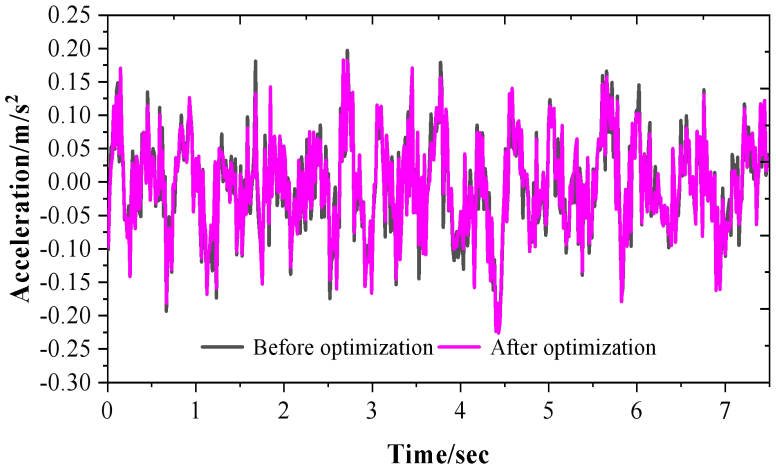

Figure 8. The acceleration curve of longitudinal vibration at driver's seat.

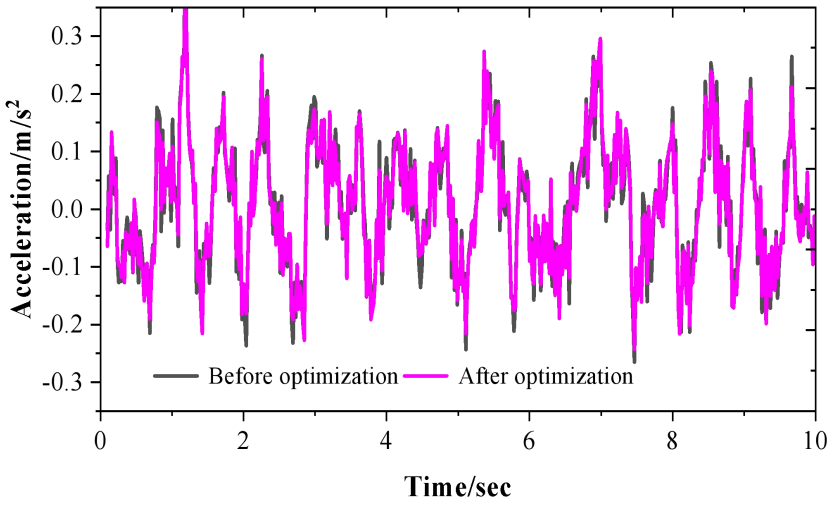

Figure 9. The acceleration curve of lateral vibration at driver's seat.

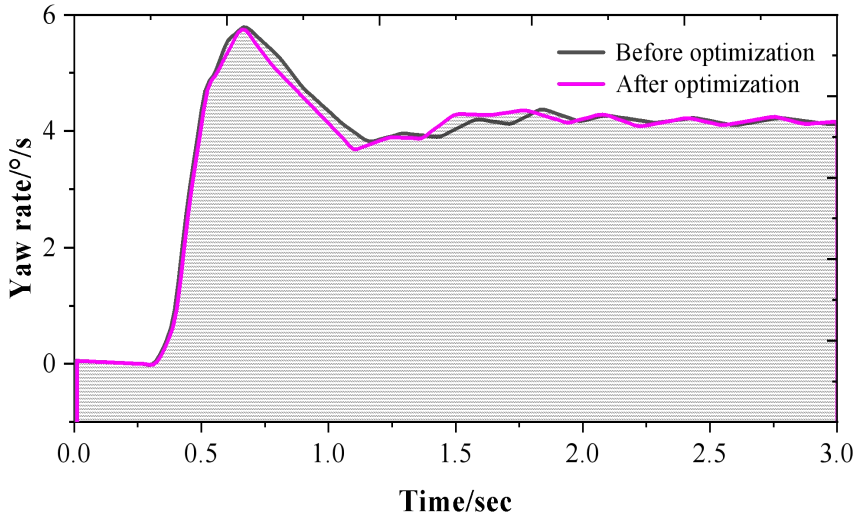

Figure 10. The yaw rate response of angular step experiment.

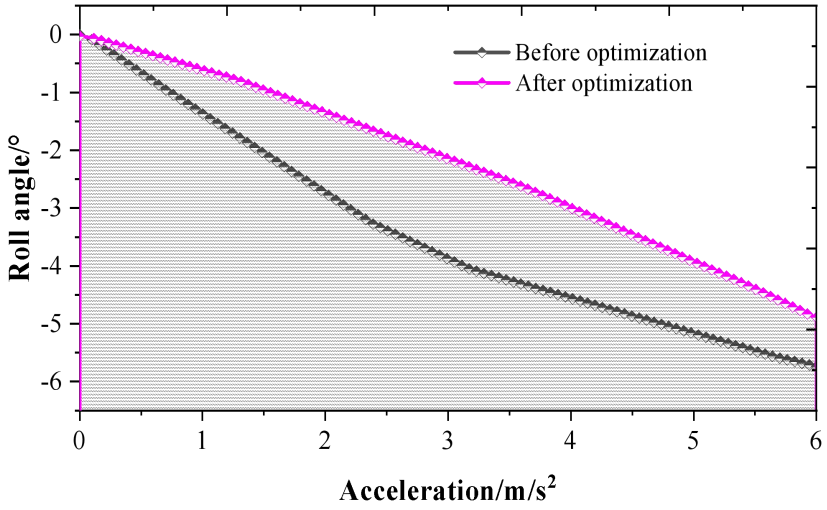

Figure 11. The vehicle roll angle of steady-state experiments.

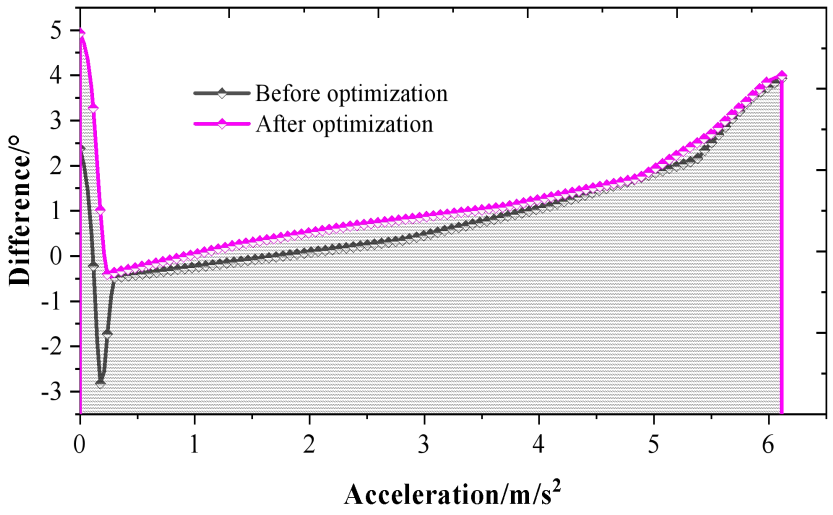

Figure 12. The difference of sideslip angle for front and rear axle.

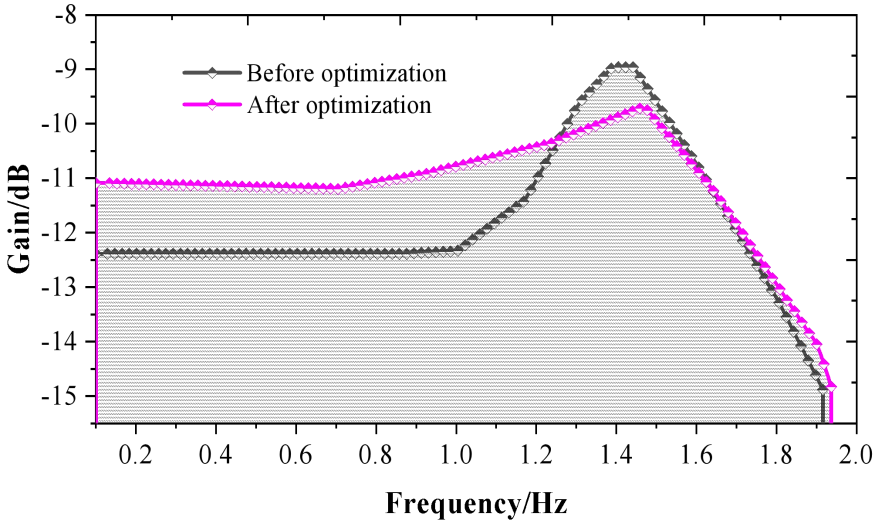

Figure 13. The frequency domain characteristics of yaw rate for angle pulse test.

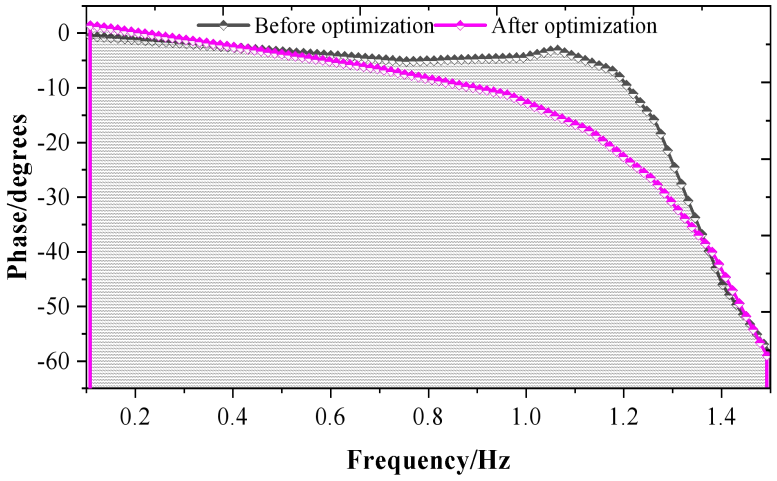

Figure 14. The time domain characteristics of yaw rate for angle pulse test.

5. Conclusion

In order to meet the high demand for automobile performance, optimal smoothness and handling stability have become the common goal pursued by today's automobile enterprises. In this paper, automobile suspension smoothness and handling stability are taken as the objective functions, a multi-objective optimization model is established, and a distributed discrete particle swarm algorithm is used to solve the problem. The optimization results show that the smoothness and handling stability of the car are improved to different degrees. Specifically, the design variables of the multi-objective optimization model after optimization are all reduced. The spring line stiffness of the front and rear suspensions is 1.54 and 1.53, the damping coefficients of the front and rear shock absorbers are 1.50 and 1.06, and the total roll Angle stiffness of the front and rear suspensions is 1.14 and 1.08. Moreover, the root mean square value of the vertical acceleration of the vehicle body and the maximum body roll Angle when the vehicle turns during driving have decreased by 4.65% and 9.27% respectively. Through the comparison of the comprehensive performance of the entire vehicle before and after optimization, it is found that the handling stability and comfort performance of the optimized vehicle have both been improved. From the experimental results, it can be seen that the research method of multi-objective optimization of automobile suspension based on distributed algorithm used in this paper has a certain degree of credibility and can provide a reference for practical situations.

This topic has made a detailed study on the design method of automobile suspension, and the proposed design method has some practical significance, but the automobile design itself is a complex discipline, and its design criteria are different due to the use of working conditions or use requirements. Therefore, in the future, it is necessary to establish a more accurate dynamic model according to the actual situation, and in the vehicle suspension optimization design to take other dynamic properties such as dynamics and throughput, as well as the vehicle to meet a variety of strength requirements and motion requirements into account, to obtain more satisfactory and accurate results.

References

1. Lukoševičius, V., Makaras, R., Rutka, A., Keršys, R., Dargužis, A., & Skvireckas, R. (2021). Investigation of vehicle stability with consideration of suspension performance. Applied sciences, 11(20), 9778.
2. Gobbi, M., Mastinu, G., Doniselli, C., Guglielmetto, L., & Pisino, E. (2021). Optimal & robust design of a road vehicle suspension system. In The Dynamics of Vehicles on Roads and on Tracks (pp. 3-22). CRC Press.
3. Chen, S. A., Cai, Y. M., Wang, J., & Yao, M. (2018). A novel LQG controller of active suspension system for vehicle roll safety. International Journal of Control, Automation and Systems, 16(5), 2203-2213.
4. Yang, W., Nong, Z., Bangji, Z., & Jie, Z. (2019). Modeling and performance analysis of a vehicle with kinetic dynamic suspension system. Proceedings of the Institution of Mechanical Engineers, Part D: Journal of Automobile Engineering, 233(3), 697-709.
5. Ferhath, A. A., & Kasi, K. (2024). The evolution of damper technology for enhanced ride comfort and vehicle handling in vehicle suspension system. International Journal of Dynamics and Control, 12(11), 3908-3946.
6. Nagarkar, M., Bhalerao, Y., Bhaskar, D., Thakur, A., Hase, V., & Zaware, R. (2022). Design of passive suspension system to mimic fuzzy logic control active suspension system. Beni-Suef University Journal of Basic and Applied Sciences, 11(1), 109.
7. Kumar, S., Medhavi, A., & Kumar, R. (2020). Active and passive suspension system performance under random road profile excitations. International Journal of Acoustics and Vibration, 25(4), 532-541.
8. Kulkarni, C. D., Sail, P. P., Kalaskar, A. V., Mitra, A. C., & Gawande, S. H. (2024). Real-time road testing and analysis of adjustable passive suspension system with variable spring stiffness. JMST Advances, 6(3), 233-246.
9. Shahid, Y., & Wei, M. (2019). Comparative analysis of different model-based controllers using active vehicle suspension system. Algorithms, 13(1), 10.
10. Attia, T., Vamvoudakis, K. G., Kochersberger, K., Bird, J., & Furukawa, T. (2019). Simultaneous dynamic system estimation and optimal control of vehicle active suspension. Vehicle System Dynamics, 57(10), 1467-1493.
11. Lan, J., & Xu, T. (2021). Adaptive Finite-Time Fault-Tolerant Control for Half-Vehicle Active Suspension Systems with Output Constraints and Random Actuator Failures. Complexity, 2021(1), 5964034.
12. Li, S., Xu, J., Gao, H., Tao, T., & Mei, X. (2020). Safety probability based multi-objective optimization of energy-harvesting suspension system. Energy, 209, 118362.
13. Li, L., Xu, L., Cui, H., Abdelkareem, M. A., Liu, Z., & Chen, J. (2021). Validation and optimization of suspension design for testing platform vehicle. Shock and Vibration, 2021(1), 7963517.
14. Sun, S., Tang, X., Yang, J., Ning, D., Du, H., Zhang, S., & Li, W. (2019). A new generation of magnetorheological vehicle suspension system with tunable stiffness and damping characteristics. IEEE Transactions on Industrial Informatics, 15(8), 4696-4708.
15. Abdelkareem, M. A., Xu, L., Zou, J., Ali, M. K. A., Essa, F. A., Elagouz, A., & Hassan, M. A. (2018). Energy-harvesting potential and vehicle dynamics conflict analysis under harmonic and random road excitations (No. 2018-01-0568). SAE Technical Paper.

16. Rostami, H. T., Najafabadi, M. F., & Ganji, D. D. (2023). Investigation of tire stiffness and damping coefficients effects on automobile suspension system. Proceedings of the Institution of Mechanical Engineers, Part D: Journal of Automobile Engineering, 237(14), 3313-3325.
17. Nagarkar, M. P., Bhalerao, Y. J., Vikhe Patil, G. J., & Zaware Patil, R. N. (2018). GA-based multi-objective optimization of active nonlinear quarter car suspension system—PID and fuzzy logic control. International Journal of Mechanical and Materials Engineering, 13(1), 10.
18. Papaioannou, G., & Koulocheris, D. (2019). Multi-objective optimization of semi-active suspensions using KEMOGA algorithm. Engineering Science and Technology, an International Journal, 22(4), 1035-1046.
19. Fossati, G. G., Miguel, L. F. F., & Casas, W. J. P. (2019). Multi-objective optimization of the suspension system parameters of a full vehicle model. Optimization and Engineering, 20(1), 151-177.
20. Ebrahimi-Nejad, S., Kheybari, M., & Borujerd, S. V. N. (2020). Multi-objective optimization of a sports car suspension system using simplified quarter-car models. Mechanics & Industry, 21(4), 412.
21. Zhang, L., Liu, J., Pan, F., Wang, S., & Ge, X. (2020). Multi-objective optimization study of vehicle suspension based on minimum time handling and stability. Proceedings of the Institution of Mechanical Engineers, Part D: Journal of Automobile Engineering, 234(9), 2355-2363.
22. Jiang, R., Jin, Z., Liu, D., & Wang, D. (2021). Multi-objective lightweight optimization of parameterized suspension components based on NSGA-II algorithm coupling with surrogate model. Machines, 9(6), 107.
23. Li, R. (2021). Multi-objective optimization of the suspension parameters in the in-wheel electric vehicle. Journal of Computational Methods in Science and Engineering, 21(4), 1013-1020.
24. Bingül, Ö., & Yıldız, A. (2023). Fuzzy logic and proportional integral derivative based multi-objective optimization of active suspension system of a 4× 4 in-wheel motor driven electrical vehicle. Journal of Vibration and Control, 29(5-6), 1366-1386.
25. Gheibollahi, H., & Masih-Tehrani, M. (2023). A multi-objective optimization method based on NSGA-II algorithm and entropy weighted TOPSIS for fuzzy active seat suspension of articulated truck semi-trailer. Proceedings of the Institution of Mechanical Engineers, Part C: Journal of Mechanical Engineering Science, 237(17), 3809-3826.
26. Llopis-Albert, C., Rubio, F., & Zeng, S. (2023). Multiobjective optimization framework for designing a vehicle suspension system. A comparison of optimization algorithms. Advances in Engineering Software, 176, 103375.
27. Nagarkar, M., Bhalerao, Y., Sashikumar, S., Hase, V., Navthar, R., Zaware, R., ... & Surner, N. (2024). Multi-objective optimization and experimental investigation of quarter car suspension system. International Journal of Dynamics and Control, 12(5), 1222-1238.
28. Verma, S., Pant, M., & Snasel, V. (2021). A comprehensive review on NSGA-II for multi-objective combinatorial optimization problems. IEEE access, 9, 57757-57791.
29. Chakraborty, S. (2022). TOPSIS and Modified TOPSIS: A comparative analysis. Decision Analytics Journal, 2, 100021.
30. Németh, B., & Gáspár, P. (2017). Nonlinear analysis and control of a variable-geometry suspension system. Control Engineering Practice, 61, 279-291.
31. Karim Afshar, K., Korzeniowski, R., & Konieczny, J. (2023). Evaluation of ride performance of active inerter-based vehicle suspension system with parameter uncertainties and input constraint via robust H∞ control. Energies, 16(10), 4099.
32. Lopes, R., Farahani, B. V., Queirós de Melo, F., & Moreira, P. M. (2023). A dynamic response analysis of vehicle suspension system. Applied Sciences, 13(4), 2127.
33. Li, Z., Zheng, L., Ren, Y., Li, Y., & Xiong, Z. (2019). Multi-objective optimization of active suspension system in electric vehicle with In-Wheel-Motor against the negative electromechanical coupling effects. Mechanical Systems and Signal Processing, 116, 545-565.
34. Cao, B., Zhao, J., Lv, Z., Liu, X., Yang, S., Kang, X., & Kang, K. (2017). Distributed parallel particle swarm optimization for multi-objective and many-objective large-scale optimization. IEEE Access, 5, 8214-8221.
35. Grotti, E., Mizushima, D. M., Backes, A. D., de Freitas Awruch, M. D., & Gomes, H. M. (2020). A novel multi-objective quantum particle swarm algorithm for suspension optimization. Computational and Applied Mathematics, 39(2), 105.
36. Wang, D., Tan, D., & Liu, L. (2018). Particle swarm optimization algorithm: an overview. Soft computing, 22(2), 387-408.
37. Hirvonen, J., & Suomela, J. (2021). Distributed algorithms 2020. Finland: Aalto University, Dec, 11, 221.
38. Ghaffari, M., & Uitto, J. (2019). Sparsifying distributed algorithms with ramifications in massively parallel computation and centralized local computation. In Proceedings of the Thirtieth Annual ACM-SIAM Symposium on Discrete Algorithms (pp. 1636-1653). Society for Industrial and Applied Mathematics.
39. Yin, L., Wang, T., & Zheng, B. (2021). Analytical adaptive distributed multi-objective optimization algorithm for optimal power flow problems. Energy, 216, 119245.
40. Romijn, T. C. J., Donkers, M. C. F., Kessels, J. T., & Weiland, S. (2018). A distributed optimization approach for complete vehicle energy management. IEEE Transactions on Control Systems Technology, 27(3), 964-980.